Transient Characterization of New Low-Pass Negative Group Delay RC-Network

Blaise Ravelo, Habachi Bilal, Sylcolin Rakotonandrasana, Mathieu Guerin, Fayrouz Haddad, Samuel Ngoho, Wenceslas Rahajandraibe

Transient Characterization of New Low-Pass Negative Group Delay RC-Network

Blaise Ravelo, *Member*, *IEEE*, Habachi Bilal, Sylcolin Rakotonandrasana, Mathieu Guerin, *Member*, *IEEE*, Fayrouz Haddad, *Member*, *IEEE*, Samuel Ngoho, Wenceslas Rahajandraibe, *Member*, *IEEE*

***Abstract*—This article studies a new resistive-capacitive (RC) topology of low-pass (LP) negative group delay (NGD) circuit. The innovative circuit theory includes the LP-NGD analysis and characterization from transfer function canonical form versus the targeted time-advance and the attenuation specifications. The new topology LP-NGD properties in both the frequency- and time-domains are introduced. The NGD value (or time-advance) and cut-off frequency in function of RC parameters, and synthesis formulas are established. The LP-NGD characterization is graphically illustrated by cartography analyses of counter-intuitive time-advance effect and NGD cut-off frequency versus RC-parameters. The LP-NGD circuit theory is transiently validated by good agreement between theory, simulation with LTspice® VXII tool and experimentation of active circuit prototype with arbitrary waveform test signal. Time-advance of some micro-seconds is demonstrated with pulse and arbitrary waveform test signals.**

***Index Terms*—Negative group delay (NGD), low-pass (LP) NGD topology, RC-network, circuit theory, time-advance.**

I. Introduction

THE SIGNAL delay effect is one of the most penalizing parameters of the communication electronic circuits [1-2]. The delay effect can be alleviated by using unfamiliar negative group delay (NGD) circuits because of its inherent time-advance signature [3-7]. For example, RF front-end oscillator and filter imperfections were compensated with NGD circuit [3]. Furthermore, medical circuits were improved by exploiting the time-advance properties of NGD circuits [4-5]. The group delay (GD) and resonance undesirable effects usually found regularly in RF system can be reduced by using different types of NGD circuit [6-7]. Nevertheless, the NGD circuit design remains, so far, an unfamiliar task for non-specialist electronic engineers. Therefore, intensive academic research work is more and more necessary for the basic and general understanding of NGD circuit design. The unfamiliar NGD behavior was initially found in optical experimentation and theory [8-9] when pulse signal was propagated in negative group velocity anomalous media. Since 1990s, progressive interests have been found in electronics engineering [10-20]. The initial study of NGD anomalous electronic circuit was based on the resonance absorption [10-11]. Then, more unfamiliar NGD theoretical approach was performed for low-frequency topologies constituted by lumped R, L and C passive components associated to operational amplifier (OA) [12-14]. It was underlined that the NGD time-advance signature does not contradict the causality [12-14] and also confirmed with pulse signal fidelity [15]. Challenging research works on compact NGD circuit design were proposed [16]. Despite the progress of research studies, the meaning, and specifications of NGD effect remain an open question for most electronic and electrical engineers. Therefore, a fundamental theory of NGD circuit was initiated by analogy with the filter [17]. Fundamental low-pass (LP) [17-18] and bandpass (BP) [17,18-20] behaviors of GD were identified with different circuit topologies. But the development and application of LP- and BP-NGD topologies necessitate further study for the non-specialist engineers to be able to use them as classical electronic functions. In the present article, an innovative circuit theory of new LP-NGD topology constituted by RC-network is investigated by means of transient characterization showing the time-advance signature. The article is organized in three different sections. Section II focuses on the new LP-NGD theorization of the innovative RC-network topology. Section III treats the validation of the LP-NGD theory with a proof-of-concept (PoC) in both frequency domain and via transient characterization. Last, Section IV is the conclusion.

This manuscript received xxx xx 2023; revised xxx xx, 2023; accepted xxx xx, 2023. Date of publication xxx xx, 2023.

(Corresponding author: Dr Habachi Bilal, E-mail: habachibilal7@gmail.com)

Blaise Ravelo is with the Nanjing University of Information Science & Technology, Nanjing, China (E-mail: blaise.ravelo@nuist.edu.cn)

Habachi Bilal, Mathieu Guerin, Fayrouz Haddad, and Wenceslas Rahajandraibe are with the Aix-Marseille University, CNRS, University of Toulon, IM2NP UMR7334, Marseille, France (E-mail: habachibilal7@gmail.com, {mathieu.guerin, fayrouz.haddad, wenceslas.rahajandraibe}@im2np.fr)

Sylcolin Rakotonandrasana is with Islamic University of Madinah, Engineering college, Madinah, Saudi Arabia (E-mail: r.sylcolin@gmail.com)

Samuel Ngoho is with Association Française de Science des Systèmes (AFSCET), 151 Bd de l'Hôpital, Paris 75013, France (E-mail: samngoho@yahoo.fr)

II. New LP-NGD Theory on RC-Network Circuit

The new LP-NGD theorization of the RC-network topology by means of voltage transfer function (TF) is developed.

A. Description of LP-NGD Specifications

One emphasizes that the first order TF is the simplest analytical model of LP-NGD topology [17]. By denoting $s=j2\pi f$ the Laplace variable, for all circuit having f-frequency dependent input and output parameters denoted by $V_{in}(s)$ and $V_{out}(s)$, the TF $T(s)=V_{out}(s)/V_{in}(s)$ is expressed by the first order system [17-18]:

$$T(s) = T_0(1+n_1 s)/(1+d_1 s) \quad (1)$$

with T_0, n_1 and d_1 are real constant. The LP-NGD TF is generally characterized by its magnitude $T(f)=|T(j2\pi f)|$ and GD:

$$GD(f) = -\partial \arg\left[T(j2\pi f)\right] / (2\pi \partial f) . \quad (2)$$

Fig. 1(a) and Fig. 1(b) represent the GD and magnitude diagrams of typical ideal LP-NGD function.

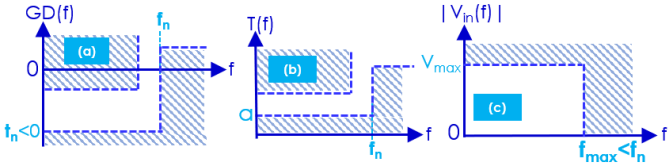

Fig. 1. (a) GD and (b) magnitude of LP-NGD function, and (c) input signal ideal diagrams.

The LP-NGD function is essentially specified by the NGD value $t_n=GD(f\approx0)<0$ and NGD cut-off frequency f_n which is the roof of equation $GD(f_n)=0$ as seen in Fig. 1(a). It is noteworthy that the LP-NGD function working frequency is not equal to $f=0$ (DC). The input signal should work as a baseband signal. In this case, the LP-NGD signature behaves with time-advance analytically illustrated by relation:

$$v_{in}(t) \approx v_{out}(t + t_n) \quad (3)$$

when $t>|t_n|$. It should be emphasized that the LP-NGD signature is obtained only with input signal v_{in} specified by maximum value V_{max} and limited spectrum baseband frequency ($|V_{in}(f)|\approx0$) as depicted by Fig. 1(c). Moreover, the magnitude at very LF can be defined by $a=|T(f\approx0)|$. For the case of passive circuit, we have $0<a<1$.

B. Canonical Standard TF of New LP-NGD Circuit Under Study

Knowing parameters t_n and a, the LP-NGD canonical form of the TF introduced in equation (1) is expressed by:

$$\begin{cases} T_0 = a \\ n_1 = t_n / (a-1) \\ d_1 = a \cdot t_n / (a-1) \end{cases} . \quad (4)$$

The associated magnitude is given by:

$$T(f) = a\sqrt{(1-a)^2 + (2\pi t_n f)^2} \,/\, \sqrt{(1-a)^2 + (2\pi a\, t_n f)^2} \quad (5)$$

By means of equation (1), the associated GD is written as:

$$GD(f) = \frac{-t_n (1-a)^2 \left[(1-a)^2 + (4\pi^2 a\, t_n^2) f^2\right]}{\left[(1-a)^2 + (2\pi a\, t_n)^2 f^2\right]\left[(1-a)^2 + (2\pi t_n)^2 f^2\right]} . \quad (6)$$

We have demonstrated the NGD cut-off frequency given by:

$$f_n = (a-1) / (2\pi \cdot t_n \sqrt{a}) . \quad (7)$$

The identified new RC LP-NGD passive topology is studied in the following subsection.

C. Analysis and Synthesis of New LP-NGD Topology

Fig. 2 depicts the LP-NGD topology constituted by resistor R and two capacitors C and D. Based on the voltage divider principle, the associated voltage TF is defined by:

$$T(s) = C(1 + R\, D\, s) / (C + D + R\, C\, D\, s) . \quad (8)$$

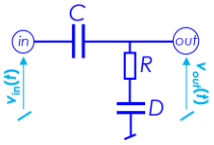

Fig. 2. RC-network new LP-NGD topology.

We analytically demonstrate from the previous equation that the GD and TF magnitude at very LF versus the considered RC-passive cell parameters are defined by, respectively:

$$T(f \approx 0) = C / (C + D) \quad (9)$$

$$GD(f \approx 0) = -D^2 R / (C + D) . \quad (10)$$

It can be underlined that the GD at very LF is unconditionally negative whatever the topological parameters. The associated cut-off frequency is given by:

$$f_n = \sqrt{C + D} / (2\pi R\, D\sqrt{C}) . \quad (11)$$

By inverting equations (9) and (10), the synthesis formulas from the targeted time-advance $t_n<0$ and attenuation a, and chosen resistor R are established. Substantially, the LP-NGD circuit capacitors can be calculated from formulas:

$$C = -a\, t_n / [R\,(1-a)^2] \quad (12)$$

$$D = t_n / [R\,(a-1)] . \quad (13)$$

In this case, the NGD value-bandwidth product $\zeta=f_n \cdot |GD(f=0)|$ is fixed and equal to:

$$\zeta = D / [2\pi\sqrt{C(C+D)}] . \quad (14)$$

The LP-NGD characterization established from these original formulas leads to the parametric analysis.

D. LP-NGD Parametric Analysis

The graphical and numerical overview on the LP-NGD behavior of the RC-network topology introduced by Fig. 2 is performed from equations (10), (12) and (13). Doing this, by fixing R=100 Ω, the capacitors were chosen in realistic range available in our laboratory, C_{min}=1 nF and C_{max}=15 nF, and D_{min}=5 nF and D_{max}=15 nF. Figs. 3 show the calculated behavioral mappings of NGD circuit characteristics represented by cartographies. As illustrated by Fig. 3(a), absolute value t_n is proportional to C and inversely proportional to D as predicted by equation (10). The same behavior is noticed by Fig. 3(b) for attenuation a. However, the NGD cut-off frequency f_n is inversely proportional to both C and D. As result, a varies between a_{min}=-2.5 dB and a_{max}=-28.3 dB with LF GD between t_{n_min}=-2.4 µs and t_{n_max}=-125 ns. Then, the cut-off frequency varies between f_{min}=104 kHz and f_{max}=780 kHz. The effectiveness of the LP-NGD topology theory is investigated with proof-of-concept (PoC) of next section.

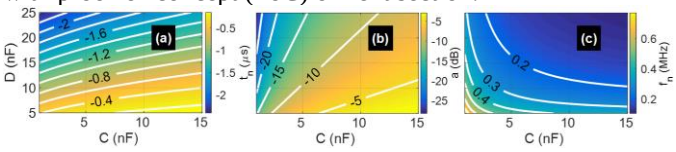

Fig. 3. Behavioral mappings of (a) t_n, (b) a and (c) f_n vs components (C,D).

III. Verification Results

Comparisons between the theoretical, simulated and experimented transient results are discussed in the following subsections. In this paper, the calculations were performed in MATLAB® environment, and the simulations were carried out by LTspice® XVII tool from Linear Technology®.

A. LP-NGD Prototype Description

The LP-NGD PoC was designed by targeted time-advance t_n=-2 µs and attenuation a_{dB}=-14 dB. By taking R=100 Ω, we have ideal and nominal values of used capacitors addressed by Table I. In order to compensate this attenuation, the LP-NGD

circuit PoC shown by schematic of Fig. 4(a) is cascaded by using non-inverting amplifier with gain $G=1/a$ or 14 dB. Therefore, by taking $R_a=R$, according to basic circuit theory, we calculate the feedback resistor $R_b=R(1/a\text{-}1)$. The printed circuit board (PCB) prototype shown in Fig. 4(b) was implemented on Cu metallized FR4-epoxy substrate by using E24-series standard RC components. During the test, the fabricated prototype was fed by symmetric power supply V_{cc+}=5 V and V_{cc-}=-5 V. The developed LP-NGD new theory effectiveness is confirmed by the following verification frequency- and especially time-domain results.

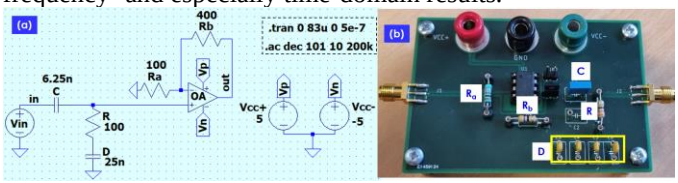

Fig. 4. LP-NGD PoC (a) LTspice® VII schematic and (b) fabricated prototype.

TABLE I
LP-NGD CIRCUIT POC PARAMETERS

Role	Nature	Parameter	Ideal value	Nominal value
Passive part	Resistor	R	100 Ω	100 Ω
	Capacitor	C	6.25 nF	6.2 nF
		D	25 nF	4×6.2 nF
Active part	OA	TL081	-	-
	Resistor	R_a	100 Ω	100 Ω
		R_b	400 Ω	390 Ω

B. AC Analysis LP-NGD Verification

The present subsection focuses on the LP-NGD circuit PoC frequency domain analysis from f_{min}=0 Hz to f_{max}=0.2 MHz. The PoC theoretical magnitude and GD were calculated from TF equation (8). Comparisons between the calculated ("Cal." plotted in red solid line) and simulated ("Sim." plotted in blue dashed line) responses were displayed in Figs. 5. A very well-correlated LP-NGD behavior is obtained. Table II summarizes the LP-NGD specifications which corresponds to the initially defined targeted ones. The notable difference between the GD responses is due to the ideal and nominal values of used capacitors during the simulation. In addition to the AC analysis, more rigorous transient validations are discussed in the following subsections.

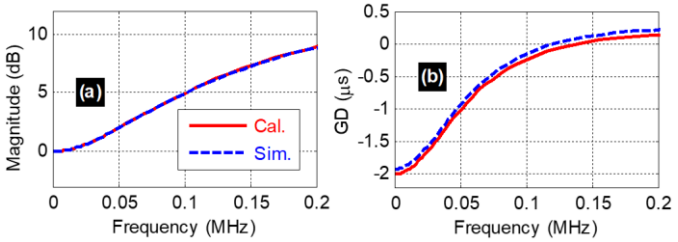

Fig. 5. Comparisons of simulated and calculated (a) magnitude and (b) *GD* of the prototype shown in Figs. 4.

TABLE II
COMPARISON OF FREQUENCY DOMAIN LP-NGD CHARACTERISTICS

Approach	t_n	f_n	$T(f\approx0)$
Theory	-2 μs	135 kHz	0.0071 dB
Simulation	-1.92 μs	122 kHz	0.0069 dB

C. Transient Validations of the New LP-NGD Theory with Gaussian Pulse Input Signal

The calibration of LP-NGD characterization is carried out by the analytical Gaussian pulse input signal to rigorously evaluate the time-advance signature. The input signal is analytically expressed as:

$$V_{in}(t)=\exp\{-5\pi^2\Delta f^2(t-t_0)^2/[\beta\ln(10)]\} \quad (15)$$

with unity amplitude V_{max}=1 V, spectral bandwidth Δf=50 kHz which is must be lower than f_n, attenuation β=20 and maximal instant time t_0=50 μs.

1) Assessment Equations of LP-NGD Temporal Result

The time-domain LP-NGD characterization is assessed by the amplitude ratio:

$$r=A_{max\_out}/A_{max\_in} \quad (16)$$

where A_{max} is the signal amplitude defined as illustrated by Fig. 6(a). The LP-NGD time-advance is assessed by the following equation system between the instant time of half amplitude maximum $v_{in}(t)=A_{max\_in}/2$ and $v_{out}(t+\Delta t)=A_{max\_in}/2$. The time advances associated to the rising and falling edge fronts are denoted $\Delta t_r\approx\text{-}t_n$ and $\Delta t_f\approx\text{-}t_n$, respectively. By denoting time sampling T_s, and k=1,2,3,…,k_{max}, the discrete input and output signals at $t=k\cdot\delta t$ under time step δt can be expressed as $v_{in,k}=v_{in}(k\cdot\delta t)$ and $v_{out,k}=v_{out}(k\cdot\delta t)$ with $k_{max}=[t_{max}/\delta t]$ ceil of real parameter $t_{max}/\delta t$. The input and output relative cross-correlation is expressed as:

$$x_c=\frac{\sum_{k=1}^{k_{max}}(v_{in,k}-\hat{v}_{in})(v_{out,k}-\hat{v}_{out})}{\sqrt{\sum_{k=1}^{k_{max}}(v_{in,k}-\hat{v}_{in})^2\times\sum_{k=1}^{k_{max}}(v_{out,k}-\hat{v}_{out})^2}} \quad (17)$$

where the averages $\hat{v}_{in}=\sum_{k=1}^{k_{max}}v_{in,k}/k_{max}$ and $\hat{v}_{out}=\sum_{k=1}^{k_{max}}v_{out,k}/k_{max}$. The application result of the cross-correlation is discussed in the next paragraph.

2) Discussion on the Advanced Behavior Gaussian Response

For this analysis, the pulse signal time duration is t_{max}=100 μs. The input signal "*In*" is plotted in black solid line. The theoretical and simulated responses are plotted in Figs. 6. The LP-NGD signature is obviously confirmed by the time-advance of output signals "$Out_{Cal.}$" from the calculation which is excellently correlated to "$Out_{Sim.}$" from LTspice® simulation.

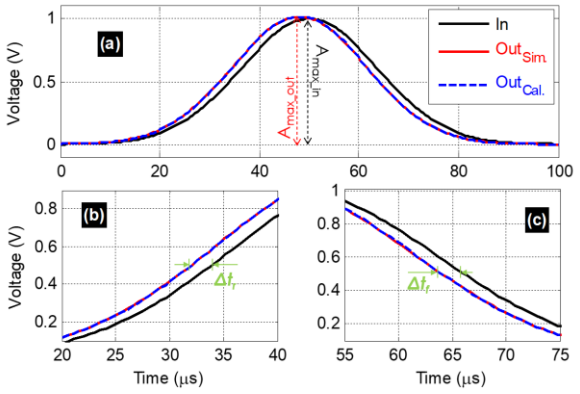

Fig. 6. LP-NGD transient responses plotted in (a) full, (b) [20 μs,40 μs] and (c) [55 μs,75 μs] time window.

TABLE III
TRANSIENT LP-NGD CHARACTERISTICS

Approach	r	Δt_r	Δt_f	x_c
Theory	1.017	-2 μs	-2 μs	99.8%
Simulation	1.015	-1.99 μs	-1.99 μs	99.3%

By means of the proposed parameters, Table III summarizes the comparison of LP-NGD transient characteristics based on relations (16) and (19) from results shown in Figs. 6. One remarks that a very good correlation between the input and

output signals showing x_c>99% is obtained. As described by the targeted specifications in subsection III-A, the theoretical and simulated time-advances are equal to -2 µs. Despite the performed transient result, further challenging validation with more practical time domain experimentation is investigated by the following subsection.

D. LP-NGD Experimental Validation with Arbitrary Waveform Signal

The performed time-domain measurement is dedicated to the characterization of LP-NGD device under test (DUT) shown by Fig. 4(b). Fig. 7(a) and Fig. 7(b) highlight the synoptic and photograph of the experimental setup carried out by the LP-NGD DUT, respectively. The employed digital oscilloscope operates with two channels. The input and LP-NGD output signals were connected to channel ① and ② for the importantly simultaneous visualization.

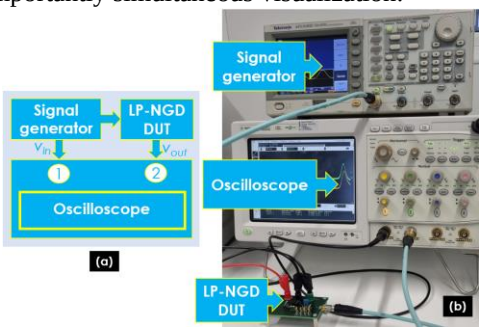

Fig. 7. LP-NGD prototype experimental test setup (a) synoptic and (b) photo.

TABLE IV
TEST EQUIPMENT SPECIFICATIONS

Description	Reference	Parameter	Value
Arbitrary function generator	Tektronix AFG3102C Dual Channel	Sampling rate	1 GS/s
		Bandwidth	100 MHz
Digital oscilloscope	Agilent infiniium MSO8104A	Sampling rate	4 GSa/s
		Bandwidth	1 GHz
		Channels	4

During the test, the arbitrary waveform signal generator was driven by external data recorded in CSV-format date to provide the input voltage. The specifications of the employed test equipment's are indicated in Table IV. The LP-NGD test was carried out within the full-time window delimited by t_{max}=83 µs as depicted by Fig. 8(a).

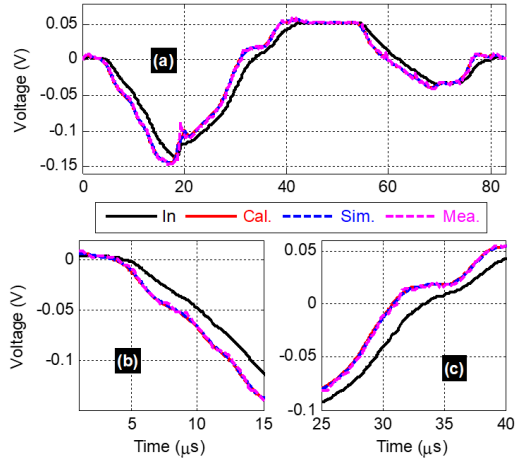

Fig. 8. Comparison of theoretical, simulated and measured transient test results plotted in (a) full, (b) [1 µs,15 µs] and (b) [25 µs,40 µs] time window of LP-NGD DUT shown in Figs. 4.

TABLE V
LP-NGD CHARACTERISTICS OF THE EXPERIMENTED LP-NGD DUT FROM ARBITRARY WAVEFORM SIGNAL RESULT SHOWN IN FIGS. 8

Approach	r	Δt_r	Δt_f	x_c
Theory	1.10	-1.95 µs	-1.92 µs	97.3%
Simulation	1.102	-1.82 µs	-1.8 µs	97.1%
Measurement	1.164	-1.63 µs	-1.614 µs	96.1%

As expected, the calculated ("Cal." plotted in red solid line), simulated ("Sim." plotted in blue dashed line) and measured ("Mea." plotted in magenta dashed line) output signals are observed. It is noteworthy that the LP-NGD DUT output is generated in advance of the input with very good agreement between theoretical, simulation and experimental results. In this case, the amplitude was assessed from relation:

$$A_{\max\{\text{in,out}\}}=\max[v_{\{\text{in,out}\}}(t)]-\min[v_{\{\text{in,out}\}}(t)]. \quad (18)$$

The averages of rise- and fall-front time advances were assessed by relations $v_{\text{out}}(t_{\text{out}})=v_{\text{in}}(t_{\text{in}})=V_T$ and $\Delta t=t_{\text{out}}-t_{\text{in}}$ for V_T={-0.075, -0.05, -0.025, 0.025} V. Table V addresses the comparison of the LP-NGD transient characteristics. Because of noise effect, the amplitude ratios and time-advances present slight differences. Nevertheless, the cross correlations expressed by equation (18) are more than 96%. The LP-NGD circuit performance can be assessed by the NGD value-product ζ. Table VI compares this work performance with the existing ones from the literature [4,12,14,18]. In addition to the benefits in terms of design simplicity and flexibility to operate up to GHz range, the original LP-NGD introduced by Fig. 2 presents NGD value-product ζ better than 234.

TABLE VI
LP-NGD PERFORMANCE COMPARISON

Ref.	[4]	[12]	[14]	[18]	This work
t_a (µs)	-5,000	-5,000	-0.8	-0.005	-1.92
f_n (kHz)	0.045	0.045	60	32,000	122
ζ	225	225	48	160	234.24
Design complexity	+	+	++	-	--
Flexibility to operate in GHz	No	No	No	Yes	Yes

IV. CONCLUSION

An innovative LP-NGD theory of RC-network circuit is developed. The specifications and properties of LP-NGD function are analytically introduced. The proposed circuit theory is established from the voltage TF via GD calculation. The LP-NGD topological synthesis relations from the targeted time-advance and attenuation are formulated. The transient validity of the new LP-NGD circuit properties is confirmed by good correlation between theory, simulation and measurement. The frequency domain validation highlights the LP-NGD behavior. In addition, transient analyses with Gaussian waveform enable to confirm the LP-NGD topology time-advance signature. Furthermore, measured transient test result inputted by arbitrary waveform signal are very well-correlated by MATLAB® calculation and LTspice® XVII simulation. As expected, the time-advance signature of about microseconds is observed. The LP-NGD function is potentially useful for the communication circuit GD effect [1-2] remedy and anticipating the future electronic device sensor and actuator defaults [21-24].

REFERENCES

[1] S.-S. Myoung, B.-S. Kwon, Y.-H. Kim and J.-G. Yook, "Effect of Group Delay in RF BPF on Impulse Radio Systems," *IEICE Tran. Commun.*, vol. 90, no. 12, Dec. 2007, pp. 3514–3522.

[2] G. Groenewold, "Noise and group delay in active filters," *IEEE Tran. CAS-I, Reg. Papers*, vol. 54, no. 7, pp. 1471–1480, Jul. 2007.
[3] C. D. Broomfield and J. K. A. Everard, "Broadband negative group delay networks for compensation of microwave oscillators and filters," *Electron. Lett.*, vol. 36, no. 23, pp. 1931–1933, 2000.
[4] C. Hymel, R. A. Stubbers and M. E. Brandt, "Temporally Advanced Signal Detection: A Review of the Technology and Potential Applications," *IEEE CAS Magazine*, vol. 11, no. 3, pp. 10-25, 3rd Quarter 2011.
[5] H. U. Voss, "Signal prediction by anticipatory relaxation dynamics," *Phys. Rev. E*, vol. 93, no. 3, (030201R), pp. 1-5, 2016.
[6] B. Ravelo, S. Lalléchère, A. Thakur, A. Saini and P. Thakur, "Theory and circuit modelling of baseband and modulated signal delay compensations with low- and band-pass NGD effects," *Int. J. Electron. Commun.* (*AEÜ*), vol. 70, no. 9, 2016, pp. 1122–1127.
[7] B. Ravelo, F. Wan, J. Nebhen, W. Rahajandraibe, and S. Lalléchère, "Resonance Effect Reduction with Bandpass Negative Group Delay Fully Passive Function," *IEEE Tran. CAS-II: Express Briefs*, vol. 68, no. 7, July 2021, pp. 2364-2368.
[8] B. Ségard and B. Macke, "Observation of Negative Velocity Pulse Propagation," *Phys. Lett. A*, vol. 109, pp. 213-216, May 1985.
[9] B. Macke and B. Ségard, "Propagation of light-pulses at a negative group-velocity," *Eur. Phys. J. D*, vol. 23, no. 1, pp. 125–141, Apr. 2003.
[10] N. S. Bukhman and S. V. Bukhman, "On the negative delay time of a narrow-band signal as it passes through the resonant filter of absorption," *Radiophysics and Quantum Electronics*, vol. 47, no. 1, 2004, pp. 66-76.
[11] M. Kandic and G. E. Bridges, "Asymptotic Limits of Negative Group Delay in Active Resonator-Based Distributed Circuits," *IEEE Tran. CAS-I: Regular Papers*, vol. 58, no. 8, Aug. 2011, pp. 1727-1735.
[12] M. W. Mitchell and R.Y. Chiao, "Negative Group-delay and 'Fronts' in a Causal Systems: An Experiment with Very Low Frequency Bandpass Amplifiers," *Phys. Lett. A*, vol. 230, no. 3-4, Jun. 1997, pp. 133-138.
[13] T. Nakanishi, K. Sugiyama and M. Kitano, "Demonstration of Negative Group-delays in a Simple Electronic Circuit," *Am. J. Phys.*, vol. 70, no. 11, 2002, pp. 1117-1121.
[14] M. T. Abuelma'atti and Z. J. Khalifa, "A new CFOA-based negative group delay cascadable circuit," *Analog. Integr. Circ. Sig. Process*., Vol. 95, 2018, pp. 351–355.
[15] H. Mao, L. Ye, and L.-G. Wang, "High fidelity of electric pulses in normal and anomalous cascaded electronic circuit systems," *Results Phys*., vol. 13, no. 102348, pp. 1–9, Jun. 2019.
[16] Y. Bai, Z. Wang, Y. M. Meng, H. Liu and S. Fang, "A Compact Dual-Band Negative Group Delay Circuit with Independently Adjustable Characteristics," *Proc. PIERS*, Hangzou, China, 25-26 Apr. 2021, pp. 1807-1811.
[17] B. Ravelo, "Similitude between the NGD function and filter gain behaviours," *Int. J. Circ. Theor. Appl.*, vol. 42, no. 10, Oct. 2014, pp. 1016–1032.
[18] F. Wan, N. Li, B. Ravelo, J. Ge, and B. Li, "Time-domain experimentation of NGD active RC-network cell," *IEEE Tran. CAS-II: Express Briefs*, vol. 66, no. 4, pp. 562–566, Apr. 2019.
[19] B. Ravelo, F. Wan, N. Li, Z. Xu, P. Thakur, and A. Thakur, "Diakoptics Modelling Applied to Flying Bird-Shape NGD Microstrip Circuit," *IEEE Tran. CAS-II: Express Briefs*, vol. 68, no. 2, Feb. 2021, pp. 637-641.
[20] F. Wan, N. Li, B. Ravelo, N. M. Murad, and W. Rahajandraibe, "NGD Analysis of Turtle-Shape Microstrip Circuit," *IEEE Tran. CAS-II: Express Briefs*, vol. 67, no. 11, Nov. 2020, pp. 2477-2481.
[21] W. Li and C. Kwan, "A Novel Approach to Sensor and Actuator Integrity Monitoring and Fault Magnitude Reconstruction," *Advances in Science, Technol. Engineering Systems Journal*, vol.2, no. 3, pp.1748, 2017.
[22] Y. -J. Liu, Q. Zeng, S. Tong, C. L. P. Chen and L. Liu, "Actuator Failure Compensation-Based Adaptive Control of Active Suspension Systems With Prescribed Performance," *IEEE Tran. Industrial Electronics*, vol. 67, no. 8, pp. 7044-7053, Aug. 2020.
[23] X. Zhang, Y. Liu, R. Rysdyk, C. Kwanand and R. Xu, "An intelligent hierarchical approach to actuator fault diagnosis and accommodation," *in Proc. 2006 IEEE Aerosp. Conf.*, Big Sky, MT, 4-11 Mar. 2006, pp. 1–5.
[24] N. F. Josso, C. Ioana, J. I. Mars and C. Gervaise, "Source motion detection, estimation, and compensation for underwater acoustics inversion by wideband ambiguity lag-Doppler filtering," *J. Acoust. Soc. Amer.*, vol. 128, no. 6, pp. 3416–3430, Dec. 2010.